Biochimie 182 (2021) 152–165

Contents lists available at ScienceDirect

Biochimie

journal homepage: www.elsevier.com/locate/biochi

Heteroarene-fused anthraquinone derivatives as potential modulators for human aurora kinase B

Mandeep Singh [a], Lakshay Malhotra [a], Md Anzarul Haque [a], Mukesh Kumar [a], Alexander Tikhomirov [b], Valeria Litvinova [b], Alexander M. Korolev [b], A.S. Ethayathulla [a], Uddipan Das [a], Andrey E. Shchekotikhin [b], Punit Kaur [a, *]

[a] Department of Biophysics, All India Institute of Medical Sciences, New Delhi, Delhi, 110029, India
[b] Gause Institute of New Antibiotics, Moscow, 11 B. Pirogovskaya Street, Moscow, 119021, Russia

ARTICLE INFO

Article history:
Received 26 July 2020
Received in revised form
10 December 2020
Accepted 29 December 2020
Available online 6 January 2021

Keywords:
Aurora kinase B
Anthraquinone
Heterocyclic compounds
Protein kinase inhibitors
Biolayer interferometry
Cell viability assay

ABSTRACT

The quest for effective anticancer therapeutics continues to be extensively pursued. Over the past century, several drugs have been developed, however, a majority of these drugs have a poor therapeutic index and increased toxicity profile. Hence, there still exists ample opportunity to discover safe and effective anticancer drugs. Aurora Kinase B (AurB), a member of the Aurora kinase family and a key regulator of mitotic cell division, is found to be frequently overexpressed in a variety of human cancers and has thus emerged as an attractive target for the design of anticancer therapeutics. In the present study, a structure-based scaffold hopping approach was utilized to modify the heterocyclic moiety of (*S*)-3-(3-aminopyrrolidine-1-carbonyl)-4,11-dihydroxy-2-methylanthra [2,3-*b*]furan-5,10-dione (anthrafuran **1**) to generate a series of heteroarene-fused anthraquinone derivatives, which were then subjected to virtual screening for the identification of potential AurB inhibitors. The obtained hits were subsequently synthesized and evaluated by using a combination of *in silico* and biophysical techniques for elucidating their *in vitro* binding and inhibition activity with recombinantly expressed AurB. Four identified hits presented an improved binding profile as compared to their parent analog anthrafuran **1**. One derivative, anthrathiophene **2** demonstrated excellent *in vitro* inhibition of AurB (7.3 μM).

1. Introduction

The side effects of chemotherapy and drug resistance, including the 'gold standard' doxorubicin, pose serious challenges to cancer patients worldwide. Altered drug responses have been implicated in raising the risk of developing secondary disorders including cancer and cardiovascular anomalies [1,2]. This emphasizes the need for exploration of newer drug targets for cancer therapy and the search for their inhibitors. The Aurora family of kinases, a family of key cell cycle regulators comprising highly conserved serine/threonine protein kinases, are being considered to be novel and effective therapeutic targets for cancer treatment [3–9].

Human cells express three different types of Aurora kinases, namely, Aurora Kinase A (AurA), Aurora Kinase B (AurB), and Aurora Kinase C (AurC). Several clinical studies have experimentally validated the overexpression of both AurA and AurB in human tumors, including breast, lung, colon, ovarian, prostate, colorectal, and pancreatic cancer [10–15]. The correlation between Aurora A/B kinase overexpression and cancer has been further substantiated over the years by analysis of numerous *in vitro* and *in vivo* expression data. Owing to this, both AurA and AurB have been projected as attractive drug targets for effective cancer treatment [16–21]. Previous studies have shown that the AurA gene is overexpressed in many tumor cells, leading to the development of new AurA inhibitors. However, recently certain studies have indicated that the overexpression of AurB, independent of AurA, is an

Abbreviations: AurB, Aurora Kinase B; AurA, Aurora Kinase A; AurC, Aurora Kinase C; anthrafuran **1**, (*S*)-3-(3-aminopyrrolidine-1-carbonyl)-4,11-dihydroxy-2-methylanthra[2,3-*b*]furan-5,10-dione; anthrathiophene **2**, 4,11-bis(2-(2-chloroacetamidino)ethyl)anthra[2,3-*b*]thiophene-5,10-dione; naphthoisatine **3**, 4,11-dimethoxy-1*H*-naphtho[2,3-*f*]isatine-5,10-dione; naphthoindole **4**, 4,11-dihydroxy-2-methyl-5,10-dioxo-*N*-(piperidin-4-yl)-1H-naphtho[2,3-*f*]indole-3-carboxamide; anthraimidazole **5**, 2-benzyl-4,11-dihydroxy-1*H*-anthra[2,3-*d*]imidazole-5,10-dione; Trp, Tryptophan; BLI, Biolayer Interferometry; MD, Molecular Dynamics.

* Corresponding author. Department of Biophysics, All India Institute of Medical Sciences, New Delhi, 110029, India.
E-mail addresses: punitkaur@aiims.edu, punitkaur1@hotmail.com (P. Kaur).

https://doi.org/10.1016/j.biochi.2020.12.024
0300-9084/

important molecular marker in determining the extent of invasiveness, recurrence, and poor prognosis of various cancerous phenotypes, reiterating its role as a critical coordinator of several events of mitosis. Consequently, research interests have now shifted to the discovery of AurB inhibitors and several pharmaceutical companies are in the process of identifying potent and selective inhibitors against it [22–30]. To date, only a handful of compounds, selectively targeting human AurB have entered clinical trials e.g. AZD1152 [30]. The increased toxicity profile of these synthetic compounds and related side effects are a source of concern which warrants the discovery and identification of novel therapeutic compounds with reduced toxicity and increased specificity.

In the era of ever-advancing targeted anticancer therapy, the anthracycline family of compounds and their analogs have proven to be promising anti-tumor agents [31–35]. However, recent studies including clinical use of these compounds have indicated their frequent association with organ toxicity (heart and bone marrow) in addition to altered drug response [36,37]. Hence, to improve the efficacy, intracellular specificity, reduce toxicity, and circumvention of drug resistance, the development of new generation of anthracycline-based drugs with their preclinical and clinical evaluation is underway [38–42]. The anthraquinone moiety of anthracyclines is largely responsible for its therapeutic properties and thus is extensively used as scaffolds for the design of various anti-cancer drugs. Recently, for the design of more effective analogs, *in silico* scaffold hopping has emerged as a significant breakthrough [43–45]. Utilizing this strategy, we identified various anthrafuran compounds (Fig. 1) that are best-in-series derivatives among anthra [2,3-*b*]furan-3-carboxamides and had a multi-target antitumor effect including the inhibition of AurB [43,46].

In this study, we have computationally designed a series of potential inhibitors of AurB, based on the chemical modifications of the anthraquinone scaffold-based compound, anthrafuran **1**. These newly designed compounds were then subjected to molecular docking and simulation studies with AurB. The top four screened compounds were subsequently synthesized and evaluated for their binding and inhibitory activity with recombinantly purified AurB. These screened heteroarene-fused anthraquinone hits were found to have enhanced binding and better inhibition profile as compared to the parent anthrafuran **1** compound.

2. Materials and methods

2.1. Protein expression and purification of AurB

The N-terminal poly Histidine tag human AurB (55–344) plasmid was procured from Nicola Burgess-Brown (Addgene plasmid #39119) [47] and subsequently expressed in *E.coli* BL21 (DE3) RIL cells. The large-scale culture was carried out in 50 μg/mL kanamycin and 35 μg/mL chloramphenicol supplemented Terrific Broth with overnight expression at 20 °C using 1 mM IPTG. Following expression, cells were harvested, centrifuged, and stored at −80 °C until further processing.

For purification, binding buffer (50 mM Tris (pH 7.5), 500 mM NaCl, 5 mM $MgCl_2$, 10 mM imidazole, 5% (v/v) glycerol and 5 mM β-mercaptoethanol) suspended cell pellet was lysed by ultrasonication and the resultant lysate was centrifuged at 21,000 g for 40 min. The clarified supernatant was loaded onto Ni-NTA column pre-equilibrated with binding buffer. The column was then washed with 10 column volumes of binding buffer containing 40 mM imidazole followed by elution with 300 mM imidazole. The protein was further purified by size exclusion chromatography using

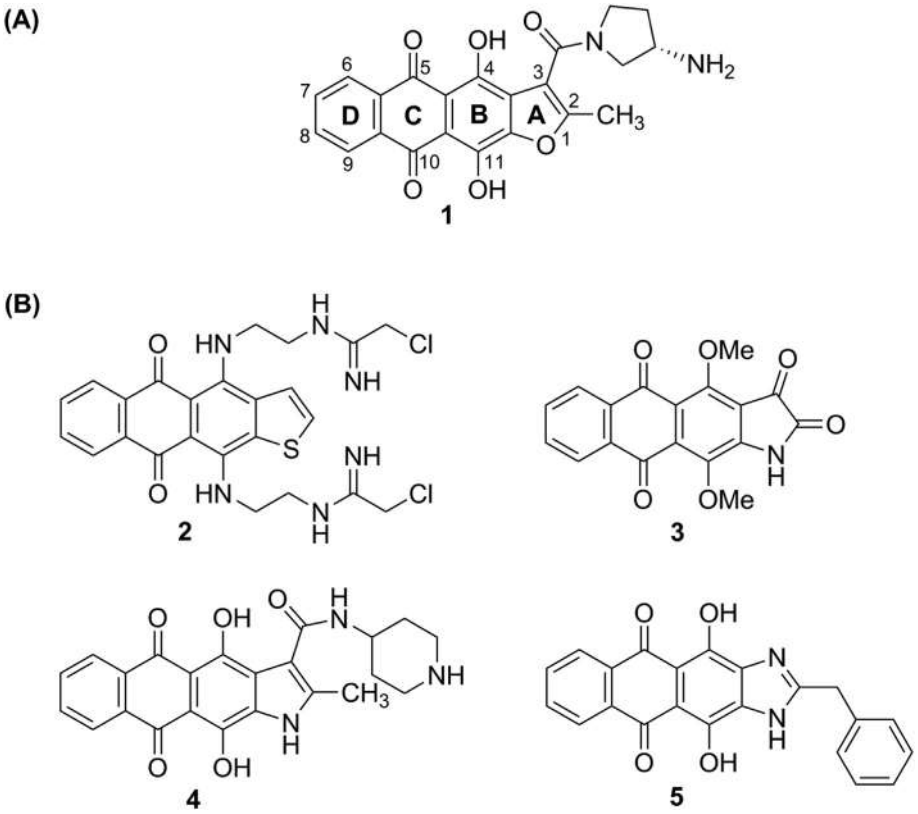

Fig. 1. (A) Structure of the parent analog anthrafuran 1 used as scaffold for subsequent modifications (B) Structure of hit heteroarene-fused anthraquinone derivatives (2–5) derived from anthrafuran 1.

Superdex 75 16/60 column with 25 mM Tris (pH 7.5), 150 mM NaCl, 5 mM $MgCl_2$, 2 mM DTT and 5% (v/v) glycerol. Protein fractions were collected and concentrated to 5 mg/mL using a 10 kDa MWCO Amicon filter for further studies. All the purification steps were performed at 4 °C.

2.2. Generation of virtual heteroarene-fused anthraquinone derivatives and molecular docking studies

A cocktail of compounds was computationally designed utilizing the planar four-ring heteroarene-fused anthraquinone scaffold of parent analog anthrafuran **1** (Fig. 1A). The shape and environment of the active site of AurB were central to the design of these molecules. Several modifications were introduced considering these properties at heterocyclic core (Het) and positions R^1, R^2, R^3 taking the parent analog anthrafuran **1** as the base scaffold (Supplementary Fig. S1**AB**). These positions involve the 4,11-hydroxy groups of furanoquinizarin derivatives and (*S*)-(3-amino) pyrrolidine cyclic diamine side chain. Previously, it has been shown that the derivatives of 3-aminomethylnaphtho [2,3-*f*]indole-5,10-dione possess high antiproliferative activity [48]. Hence, the carbonyl group of the carboxamide fragment of anthrafurandione-3-carboxamides was also modified. These modifications of the scaffold (Supplementary Table S1**)** created a library of over 2 million chemical structure derivatives**.** All the generated compounds were utilized for primary virtual screening and computational evaluation for their drug-likeness potential and ADMET profile. The top 20 screened candidates were further evaluated based on binding energy and favorable interactions with target AurB resulting in the filtering out of four hit compounds **2**–**5** (Fig. 1B).

For docking studies, the three-dimensional coordinates of Human AurB with co-crystallized ligand VX-680 were retrieved (PDB ID: 4AF3) [47]. Docking studies of screened heteroarene-fused anthraquinone hits with target AurB was performed after considering the binding site based on active site residues and the position of co-crystallized inhibitor (VX-680). The target protein was prepared for docking by Protein Preparation wizard (Schrodinger LLC) [49]. Two-dimensional diagrams of screened derivatives were drawn using the program Marvin Sketch [50] and their corresponding 3D coordinates were generated through OPENBABEL software [51]. These compounds were then further optimized using LigPrep [52]. Multiple grids (5–15 Å) that defined a cube where the ligand is proposed to bind were generated with the centroid of the co-crystallized ligand. Glide (grid-based ligand docking) was utilized for docking as it approximated a complete search of the conformational, orientation, and positional space of the ligand in the receptor [53]. The docked complexes were then analyzed for their potential binding mode and protein-ligand interactions. The docked complex with the best pose was refined by energy minimization to get rid of any steric clash. Further, the minimized docked complexes were incorporated into the Prime-MM-GBSA module to elucidate their respective binding free energy scores [54]. The top docked pose based on binding free energy and interactions with AurB were selected for the confirmation of binding complex stability through Molecular Dynamics (MD) simulation.

MD simulation was carried out to assess the dynamic stability of the protein-ligand complex for the specified time scales (50 ns) using DESMOND [55]. NPT ensemble with temperature 300 K and

Table 1
Non-covalent interactions of hits within 4 Å with Aurora B. Residues involved in hydrogen bonding interactions are highlighted in bold.

Compounds	Structure	MM/GBSA binding energy (kcal/mol)	Interacting residues (within 4 Å)
2	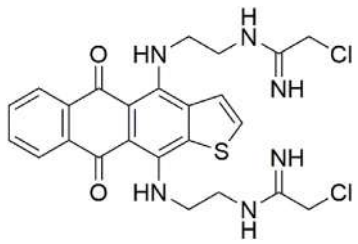	−60.7	Leu83, Gly84, Lys85, Phe88, Tyr156, Ala157, **Arg159**, Gly160, **Glu161**, Lys164, Glu 165, **Glu204**, Leu207
3	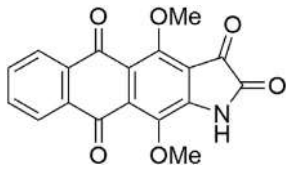	−45.5	Leu83, Phe88, Val91, Ala104, **Lys106**, Leu138 Leu154, Glu155, Tyr156, Ala157, Gly160, Glu161, Glu204, Leu207
4		−47.2	Leu83, Gly84, Lys85, Phe88, Leu138, Leu154, Glu155, Tyr156, **Ala157**, Pro158, Gly160, Glu161, Leu207
5	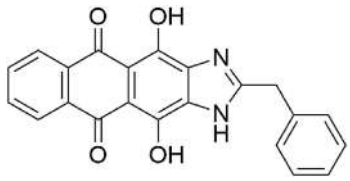	−34.1	Leu83, Val91, Ala104, Glu155, Tyr156, **Ala157**, Pro158, Arg159, Gly160, Glu161, Lys164, Leu207

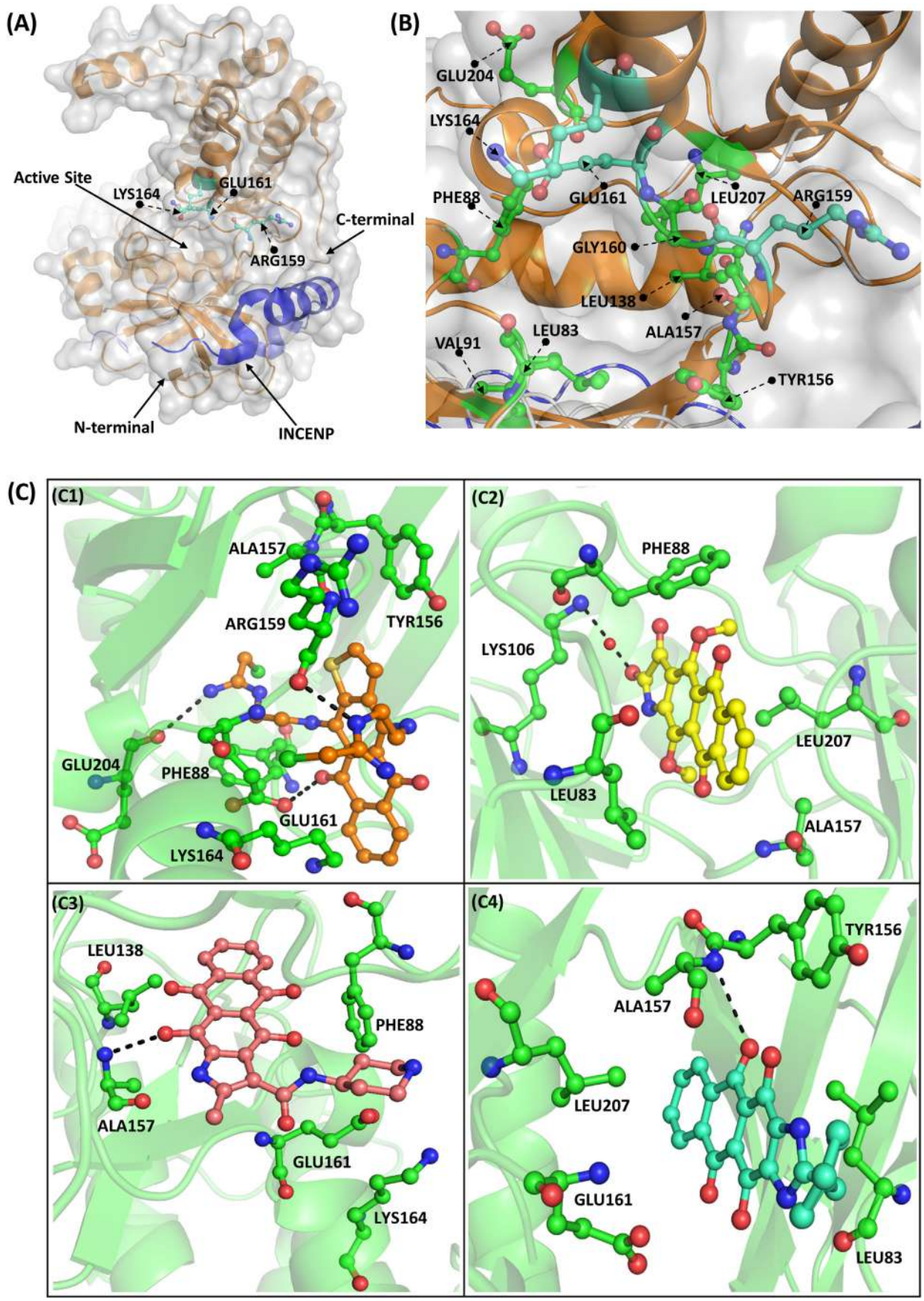
(A)
Active Site
LYS164
GLU161
ARG159
C-terminal
N-terminal
INCENP
(B)
GLU204
LYS164
PHE88
GLU161
LEU207
ARG159
GLY160
LEU138
LEU83
ALA157
VAL91
TYR156
(C)
(C1)
ALA157
ARG159
TYR156
GLU204
PHE88
GLU161
LYS164
(C2)
PHE88
LYS106
LEU207
LEU83
ALA157
(C3)
LEU138
PHE88
ALA157
GLU161
LYS164
(C4)
TYR156
ALA157
LEU207
GLU161
LEU83

pressure 1 bar was applied on all runs with relaxation time for each complex set to 1ps. The OPLS2005 force field parameters were used for all the simulation runs. The long-range electrostatic interactions were calculated using the particle mesh EWALD method. The system was prepared prior to simulation using the System builder tool of Desmond. The boundary condition was defined by setting a 10 Å × 10 Å x 10 Å orthorhombic box around the protein with the cut off radius of Coulomb interactions at 10 Å. The system was solvated using the Simple Point Charge (SPC) solvent model and set up in a 0.15 M NaCl solution to mimic the physiological conditions. The stability of MD simulations was checked by monitoring the overall RMSD of the protein-ligand complex.

2.3. Synthesis of compounds

NMR spectra were recorded on a Varian Mercury 400 Plus instrument operated at 400 MHz (^{1}H NMR) and 100 MHz (^{13}C NMR). Chemical shifts were measured in DMSO-d_6 using tetramethylsilane as an internal standard. Analytical TLC was performed on Silica Gel F_{254} plates (Merck). Column chromatography was performed using SilicaGel Merck 60. Melting points were determined using a Buchi SMP-20 apparatus and are given uncorrected. High-resolution mass spectra were recorded with electron spray ionization on a Bruker Daltonics microOTOF-QII instrument. HPLC was performed using a Shimadzu Class-VP V6·12SP1 system, A: 0.01 M H_3PO_4 pH = 2.6; B: MeCN. All solutions were dried over Na_2SO_4 and evaporated at a reduced pressure using IKA RV 10 rotary evaporator at < 45 °C. All products were vacuum dried at room temperature. All solvents, chemicals, and reagents were obtained from Sigma-Aldrich, St. Louis, MO unless specified otherwise, and used without purification.

Compounds **1**–**3** were synthesized according to the previously developed methods [43,56,57]. The purity of all samples was ≥95%.

4,11-Dihydroxy-2-methyl-5,10-dioxo-N-(piperidin-4-yl)-5,10-dihydro-1H-naphtho [2,3-f]indole-3-carboxamide (naphthoindole **4**).

A mixture of acid **6** (0.10 g, 0.3 mmol) and thionyl chloride (0.2 mL, 2.8 mmol) in benzene (10.0 mL) was boiled for 30 min, cooled to room temperature and evaporated under vacuum [58]. The resulting acyl chloride was immediately used at the next steps without purification. To a suspension of crude acyl chloride in anhydrous chloroform (5 mL) a solution of *tert*-butyl 4-aminopiperidine-1-carboxylate (80 mg, 0.4 mmol) and pyridine (0.1 mL, 1.2 mmol) in anhydrous chloroform (5 mL) was added. The mixture was refluxed for 5 min, diluted with chloroform (20 mL), washed with aqueous HCl (0.3 M) and water, then dried and evaporated. The residue was purified by column chromatography on a silica gel using chloroform-methanol (10:0 → 10:1) as the eluent. The red solid obtained after evaporation was dissolved in hot chloroform (10 mL). Methanesulfonic acid (0.2 mL, 3.1 mmol) was added, the mixture was stirred overnight and evaporated. The residue was dissolved in boiling water (1 mL), filtered, and the product was precipitated with acetone-ether (4:1). The red solid was collected by filtration, washed with acetone, Et_2O, n-hexane and dried. The yield of naphthoindole **4** was 0.10 g (66%) as a red solid, mp > 250 °C. HPLC (LW = 260 nm, gradient B 20 → 60% (30 min)) t_R = 17.6 min, purity 99%. ^{1}H NMR (400 MHz, DMSO-d_6) δ 14.91 (s, 1H, OH); 14.75 (s, 1H, OH); 13.12 (s, 1H, NH); 9.41 (d, 1H, J = 7.0, CONH); 8.59 (br s, 1H, NH_2); 8.38 (br s, 1H, NH_2); 8.12–8.10 (m, 2H, 6,9-H); 7.79–7.77 (m, 2H, 7,8-H); 4.03–4.00 (m, 1H, CH); 3.35–3.33 (m, 2H, $(CH_2)_2NH$); 3.17–3.12 (m, 2H, $(CH_2)_2NH$); 2.42 (s, 3H, CH_3); 2.36 (s, 3H, SCH_3); 2.13–2.10 (m, 2H, CH_2); 1.79–1.74 (m, 2H, CH_2). ^{13}C NMR (100 MHz, DMSO-d_6) δ 177.7 (C═O); 169.8 (C═O); 164.4 (N–C═O); 164.3 (C); 161.9 (C); 144.4 (C); 132.0 (2CH); 130.8 (C); 130.0 (C); 129.9 (C); 124.8 (CH); 124.6 (CH); 122.5 (C); 115.4 (C); 106.1 (C); 105.6 (C); 43.0 (CH); 41.7 ($2CH_2NH_2$); 39.7 (SCH_3); 27.7 ($2CHCH_2$); 12.9 (CH_3). HRMS (ESI) calculated for $C_{23}H_{21}N_3O_5$ $[M+H]^+$: 420.1559, found 420.1530 (Supplementary Fig. S2).

2-Benzyl-4,11-dihydroxy-1H-anthra [2,3-d]imidazole-5,10-dione (anthraimidazole **5**).

A mixture of 2,3-diaminoquinizarine **7** (0.50 g, 1.85 mmol) and phenylacetic acid (5.00 g, 37 mmol) was stirred at 170 °C under argon for 20 min and poured into water [59]. The produced mixture was basified with aqueous NaOH (5 M) to pH = 8, the solid was filtered, washed with water and dried. The residue was recrystallized from nitrobenzene. The yield of anthraimidazole **5** was 0.45 g (69%) as a brown solid, mp > 250°C. HPLC (LW = 260 nm, gradient B 20 → 60% (30 min)) t_R = 17.6 min, purity 99%. ^{1}H NMR (400 MHz, DMSO-d_6) δ 14.55 (s, 2H, OH); 13.95 (br s, 1H, NH); 8.33–8.31 (m, 2H, 6,9-H); 7.93–7.90 (m, 2H, 7,8-H); 7.36–2.25 (m, 5H, Ph); 4.24 (s, 2H, CH_2). ^{13}C NMR (100 MHz, DMSO-d_6) δ 177.4 (2C = O); 156.7 (C-2); 136.4 (C^{Ph}); 133.3 (2CH, C); 132.1 (2C); 128.5 (C, $2C^{o-Ph}$); 128.2 ($2C^{m-Ph}$); 126.4 (C, C^{p-Ph}); 125.6 (2CH, C); 106.5 (2C); 34.2 (CH_2). HRMS (ESI) calculated for $C_{22}H_{15}N_2O_4$ $[M+H]^+$: 371.1026, found 371.1046 (Supplementary Fig. S3).

2.4. In vitro fluorescence binding

In vitro binding interaction of AurB with synthesized hits was studied by monitoring tryptophan quenching. Experiments were carried out with 1 cm path length quartz cuvette on Jasco Spectrofluorimeter (FP-6200) at pH 7.5 and 25 ± 0.1°C using a thermostated water circulator. Ligands were dissolved in DMSO and diluted to working concentration in TBST buffer (50 mM Tris, 150 mM NaCl, 1 mM DTT, 0.01% Tween 20). The fluorescence emission experiment was conducted in the presence of each synthesized hit compound **(2–5)** and parent anthrafuran **1** over a concentration range of 1–200 μM. The emission spectra of AurB in the presence of different concentration range of ligands were collected in the wavelength range 300–400 nm after excitation of tryptophan (Trp221, Trp257, and Trp326) at 280 nm. A non-hydrolyzable analog of ATP, AMP-PNP was then utilized to determine its competitiveness with ATP. The competition assay was carried out in the presence of different concentrations of compounds **1**–**5** separately to evaluate the change in binding prowess of AMP-PNP with AurB by following the protocol of Eathiraj and Ashwell [60]. A complex of AurB (1 μM) was prepared at varying concentrations (6.25, 25, 50, and 100 μM) of the compounds **1**–**5** separately and incubated for 1 h. In the same samples, AMP-PNP were serially diluted (0 μM–200 μM). The competition between the compounds and AMP-PNP was observed by comparing the binding affinity of AMP-PNP with AurB alone and with the complex of AurB and compounds **1**–**5** individually. For all the experiments, the excitation and emission slit width were both set at 5 nm. Spectra were taken for compounds in assay buffer without protein for baseline correction. Parallel buffer controls were measured to correct the background fluorescence quenching caused by the

Fig. 2. (A) Cartoon structure of AurB (light brown) with INCENP (blue) together with the surface representation of the protein indicating the active site pocket (black arrow) and active site residues (cyan) important for its selective inhibition. (B) Surface representation of the binding region of AurB pinpointing the active site residues (cyan; ball and stick) and other interacting residues (green; ball and stick) with the hit compounds 2–5. (C) MD simulation refined docked poses of hit compounds (C1) Anthrathiophene 2 (orange), (C2) Naphthoisatine 3 (yellow), (C3) Naphthoindole 4 (deep salmon), (C4) Anthraimidazole 5 (cyan), with AurB (green). The compounds and the side-chain of interacting residues of AurB are represented in ball and stick and hydrogen-bonded interactions are shown by black dashed lines.

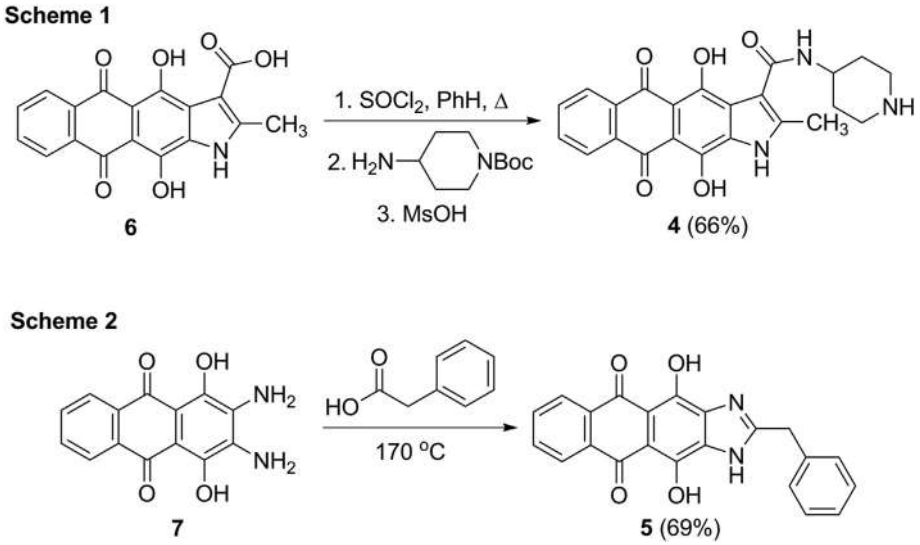

Fig. 3. Scheme 1 – Schema for synthesis of 4,11-dihydroxy-2-methyl-5,10-dioxo-N-(piperidin-4-yl)-1H-naphtho [2,3-f]indole-3-carboxamide (naphthoindole 4); Scheme 2 – Schema for synthesis of 2-benzyl-4,11-dihydroxy-1H-anthra [2,3-d]imidazole-5,10-dione (anthraimidazole 5).

buffer if any. The results were analyzed by fitting the saturation curve in the nonlinear equation (1) in the Sigma curve fitting wizard for the determination of K_d value for all the compounds.

$$f = a+(b-a)*((x+0.5+K_d)-((x+0.5+K_d)\text{^}2-2*x)\text{^}0.5) \quad (1)$$

2.5. Biolayer interferometry (BLI) assay

The binding interactions between AurB and the synthesized compounds **1**–**5** were further monitored in real-time by performing BLI assay with the Octet-Red 96 system (FortéBio Inc., USA) [61]. His tagged AurB was first captured onto Ni charged NTA sensors and the unbound AurB was washed using the assay buffer (25 mM HEPES pH 7.4, 200 mM NaCl, and 0.01% Tween 20 supplemented with 0.2 mg mL^{-1} BSA). To initiate association, AurB loaded sensors were then incubated in the presence of a serially diluted concentration of each analyte (synthesized compounds) at 1000 rpm for 180–360 s till saturation was achieved in independent binding experiments. The dissociation of the protein-compound complex was then monitored by dipping sensors in assay buffer alone for the same period. A reference sensor without bound AurB was simultaneously subjected to the same protocol as the NTA sensors loaded with the ligand for baseline correction. The experiments were carried out in triplicates at a constant temperature of 25 °C in Greiner 96 well black microwell plates. The real-time data were analyzed and K_d values were determined using Curve fit (1:1, association; dissociation) model in the Octet® software.

2.6. ADP-Glo™ kinase assay

The inhibitory activity of hit heteroarene-fused anthraquinone derivatives with AurB was assessed by performing the ADP-Glo™ kinase assay according to the manufacturer's protocol [62]. Prior to the inhibition experiments, a kinase titration experiment was done to standardize the optimal amount of AurB required for the subsequent dose-response curve. The lab synthesized heteroanthraquinone hits were then incubated with recombinant human AurB for few hours at 25 °C. The inhibition assay was carried out in 96-well solid white, round bottom plate in a volume of 20 μL containing 9 nM/well AurB, 0.1 μg/μL MBP substrate, 5 μL of serially diluted compound, and 10 μM ATP. The reactions in each well were started by the addition of ATP immediately and the reaction plate was incubated for 60 min at 25 °C. 20 μL of ADP Glo™ reagent was then added to each well and further incubated for 40 min at 25 °C. This step converts ADP into ATP and depletes the unused ATP. Finally, 40 μL of kinase detection reagent was added in each well and the resultant luminescence was recorded after 30 min of further incubation at 25 °C with Spectramax® i3x Multi-Mode Microplate reader (Molecular Devices). The resultant decrease in luminescent intensity was directly correlated with the inhibition efficiency of each hit by Curve fitting using GraphPad Prism® sigmoidal dose-response ((log) vs three parameters) software.

2.7. MTT assay

The cytotoxic effect of synthetic compounds **2**–**5** and parent anthrafuran **1** was determined on two different AurB overexpressing Saos-2 (osteosarcoma) and MDA-MB-453 (breast sarcoma) cell lines (National Centre For Cell Science (NCCS), Pune, India) along with the non-cancerous HEK-293T cell line as control. In each well around 8000 cells were seeded in a 96-well plate along with 200 μL of complete DMEM media (Gibco, Thermo Fisher Scientific) containing 10% FBS and 1% Antibiotic and Antimycotic. The media was discarded on the next day and cells were treated with 200 μL of different concentrations (1, 3.5, 7, 10, 15, 20, 30, 40, 50, 75, and 100 μM) of compounds along with control in 6 replicates and then cells were incubated for 24 h in CO_2 incubator. After incubation, 20 μL of 5 mg/mL MTT solution prepared in 1X PBS was added and the cells were again incubated for 4 h. Further, the wells were decanted and Formazone crystals were solubilized in 80 μL DMSO and kept cells at room temperature for 15 min. Finally, the optical densities were measured in Spectramax i3x at 575 nm.

The cytotoxicity was calculated using the formula:

$$\%\ \text{cytotoxicity} = (1-(\text{absorbance of test}/\text{absorbance of control})) \times 100$$

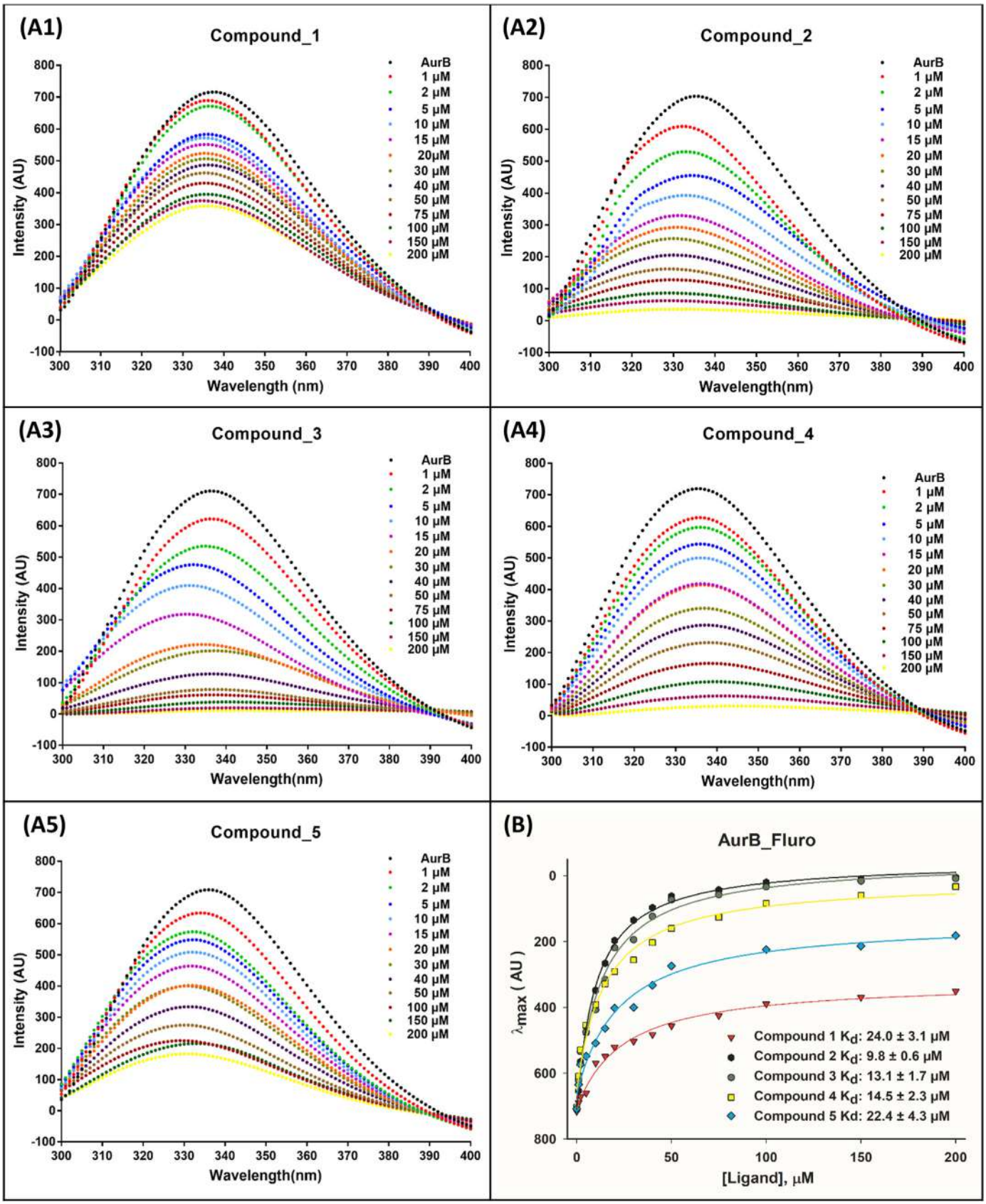

Fig. 4. Binding studies of hit compounds with AurB using fluorescence spectroscopy. (A1-A5) The emission spectra of AurB (3.0 μM) in the presence of different concentrations of compounds 1–5 (0–200 μM) was collected in the wavelength range 300–400 nm after excitation of the tryptophan residues (Trp221, Trp257, and Trp326) at 280 nm. (B) The values of fluorescence intensity at 338 nm plotted as a function of ligand concentration to determine the binding parameters.

Table 2
Binding affinity (K_d, μM) of heteroarene-fused anthraquinones 1–5 with Human AurB.

Compounds	Biolayer Interferometry (K_d, μM)	Fluorescence Spectroscopy (K_d, μM)
1	29.0 ± 0.6	24.0 ± 3.2
2	4.2 ± 0.1	9.8 ± 0.6
3	14.5 ± 0.3	13.1 ± 1.7
4	14.3 ± 0.3	14.5 ± 2.3
5	23.7 ± 1.1	22.4 ± 4.3

3. Results

3.1. Identification of anthrafuran analogs by assessing protein-ligand interactions

The library of heteroarene-fused anthraquinone derivatives was designed with substitutions at different positions of the ring keeping parent compound anthrafuran **1** (Fig. 1A) as the reference molecule. The core of all these compounds comprised the initial scaffold which is a planar polycyclic molecule enabling it to comfortably sit in the non-polar binding pocket of AurB. All the designed structures were subsequently docked into the active site of AurB. The protein-ligand complexes were analyzed for their binding interactions. The molecular docking resulted in filtering out four compounds **2**–**5** (Fig. 1B) which gave better binding energy and molecular interactions than the parent compound anthrafuran **1** [43]. The Molecular Mechanics/Generalized Born Surface Area (**MM**/**GBSA**) binding energy of all the obtained hits are summarized in Table 1.

The docking calculations were followed by MD simulation of each AurB-hit complex to evaluate the stability and the flexibility of the designed hits. The ability of the complex to remain bound in the presence of an explicit solvent was also assessed. The RMSD fluctuations of the atomic positions of both protein and each bound ligand were between 1 and 3 Å for a notably large part of the simulation time indicating the stability of the complex in the active site**.** The active site residues and amino acid residues located in the hydrophobic pocket situated near the active site of the protein (Fig. 2AB) **were** majorly observed to interact with the compounds **2**–**5**.

The 4,11-bis(2-(2-chloroacetamidino)ethyl)anthra [2,3-*b*]thiophene-5,10-dione (anthrathiophene **2**) has the largest side-chain amongst the four derivatives **2**–**5**. Its core scaffold reorients itself to adjust the large substituent in the binding pocket enabling strong hydrophobic interaction of 11-((2-chloroacetamidino)ethylamino) arm with Phe88. Additionally, the thiophene ring of anthrathiophene **2** is involved in hydrophobic interactions with Tyr156 and Ala157. The hydrophobic core of anthrathiophene **2** is surrounded by the side chains of hydrophobic residues Leu83, Gly84, Gly 86, Gly 89, Phe88, Val91, Leu138, Leu154, Tyr156, Ala157, Gly160, Leu207 as also observed for other hit derivatives.

The positively charged nitrogen atom of 11-((2-chloroacetamidino)ethylamino) and 4-((2-chloroacetamidino)ethylamino) arm were involved in stable hydrogen-bonded interaction with the main chain carbonyl oxygen of Glu204 and Arg159 respectively. Another strong hydrogen bond was observed between the 10-carbonyl oxygen of the anthraquinone moiety and the Glu161 side-chain. Significant cation-π interaction between the primary benzene ring of the heteroarene-fused anthraquinone core and the main chain nitrogen of Lys164 majorly contribute to the stabilization of the ligand-protein complex in the binding pocket of AurB (Fig. 2 **C1**).

The binding mode of 4,11-dimethoxy-1*H*-naphtho [2,3-*f*]isatine-5,10-dione (naphthoisatine **3**) in the ATP binding pocket of AurB was found to be similar to the co-crystallized inhibitor, VX-680, which targets the ATP binding pocket of AurB and overlapped well with its pyrazole-benzimidazole core [47]. The polycyclic system of naphthoisatine **3** was observed to be involved in several stable van der Waals interactions with hydrophobic side-chains of surrounding amino acids at the binding pocket. The carbonyl oxygen of the anthraquinone core formed a strong hydrophobic interaction with the phenyl residue of Phe88. Additional interactions were observed between the methoxy groups of naphthoisatine **3** and the side-chain carbon atoms of Leu207. The 2-carbonyl oxygen of the pyrrole-2,3-dione ring of naphthoisatine **3** revealed water-assisted hydrogen bonding interaction with the side-chain amino group of Lys106 (Fig. 2C2).

The predicted binding mode of 4,11-dihydroxy-2-methyl-5,10-dioxo-*N*-(piperidin-4-yl)-1*H*-naphtho [2,3-*f*]indole-3-carboxamide (naphthoindole **4**) was quite similar to anthraimidazole **5** with the planar fragment nearly stacking with the docked orientation of each other. The 11-hydroxy oxygen of the anthraquinone core was involved in a stable hydrogen bond main chain nitrogen of Ala157 (Fig. 2C3). Further stability to the complex was provided through van der Waals interactions notable being the side-chain of Leu138 with the aromatic **D** ring of the tetracyclic system of the ligand and phenyl carbon of Phe88 with the side-chain of carboxamide piperidine substituent.

For 2-benzyl-4,11-dihydroxy-1*H*-anthra [2,3-*d*]imidazole-5,10-dione (anthraimidazole **5**), the predicted orientation was found to be reasonably similar to naphthoisatine **3**. The polycyclic core of anthraimidazole **5** was observed to be completely immersed in the hydrophobic cavity of the ATP binding pocket and was stabilized by the side-chain residues of Leu83, Phe88, Leu138, and Leu207. The 10-quinone oxygen of anthraimidazole **5** formed a strong hydrogen bond with the Ala157 amino group, further stabilizing the complex (Fig. 2 **C4**).

The binding modes of two derivatives, naphthoindole **4** and anthraimidazole **5** are comparable to the parent heteroarene-fused anthraquinone anthrafuran **1** including similar hydrogen-bonding interactions with Ala157 [43]. Derivative anthrathiophene **2** has a bulky substituent, and formed hydrogen bonding interaction with Arg159, Glu161, and Glu204 and additional strong cation-π interaction with Lys164 which can be attributed to the stabilization of the protein-ligand complex. The derivative, naphthoisatine **3,** was stabilized through a water-mediated hydrogen bond. The simulation refined non-covalent interactions for each hit is summarized in Table 1. For experimental validation of the proposed molecular models, synthesis and biological estimation of derivatives **2**–**5** and parent anthrafuran **1** were carried out.

3.2. Chemistry behind the synthesized hit compounds

Compounds **1**–**3 (Fig. 1AB)** were prepared following the previously developed methods [43,56,57], while for the derivatives naphthoindole **4** and anthraimidazole **5** we have developed new synthetic schemes. The starting compounds **6** and **7** for target transformations were prepared in accordance with previously described procedures [58,59]. Naphthoindole **4** was obtained from the corresponding carboxylic acid applying the same method used

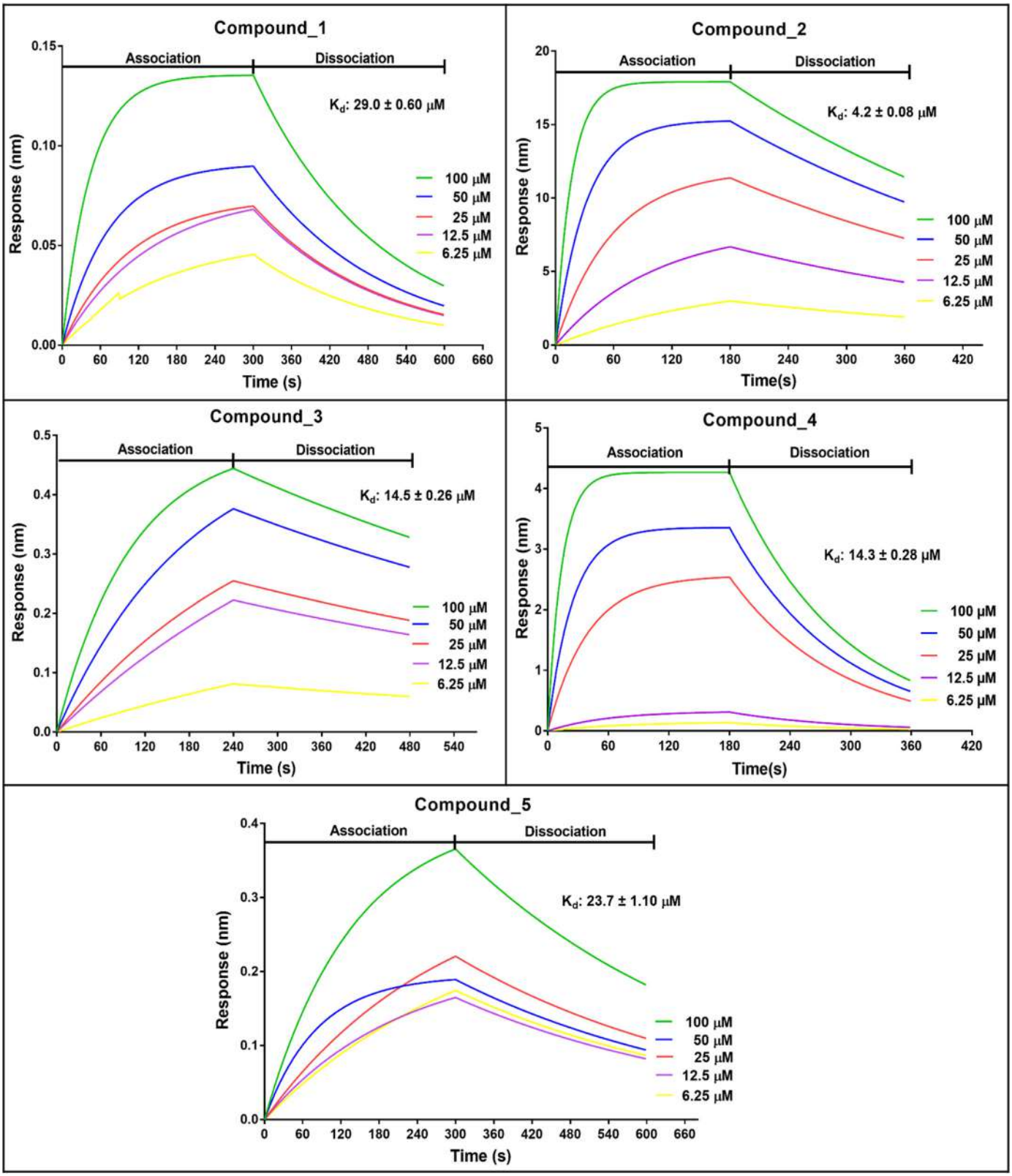

Fig. 5. BLI experiments plotted on a linear scale indicate the association and dissociation curves at varying concentration for compounds 1–5. The human AurB protein (50 μg/mL) was immobilized on the NTA sensor and dipped in each compound at different concentrations till saturation. The compound concentration of 100 μM (green), 50 μM (blue), 25 μM (red), 12.5 μM (purple) and 6.25 μM (yellow) were used for each compound.

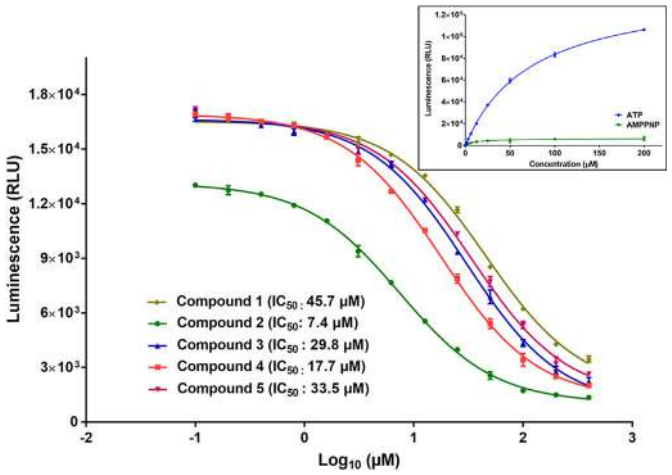

Fig. 6. Dose-response curve was created using 9 nM of AurB to determine the potency of heteroarene-fused anthraquinone derivatives 1–5. Curve fitting was performed using Graphpad Prism® sigmoidal dose-response ((log) vs three parameters) software. Data points are the average of two independent determinations with the error bars indicating ± S.D. IC_{50} values for each tested compound are given with respective colors. Inset: Kinase assay was performed for AurB (9 nM) and MBP substrate (0.1 μg/mL) with various concentrations of ATP and AMP-PNP (0–200 μM) to check the hydrolysis of AMP-PNP to ADP in comparison to ATP. Significant luminescence was recorded for each increase of ATP concentration but insignificant luminescence was detected in the reaction involving AMP-PNP which shows the failure of hydrolysis of AMP-PNP and non-release of gamma phosphate and formation of ADP.

for the synthesis of parent analog anthrafuran **1**. In particular, boiling of naphtho [2,3-*f*]indole-3-carboxylic acid **6** with $SOCl_2$ formed acid chloride which was used for acylation of 1-Boc-4-aminopiperidine (Fig. 3; Scheme 1). Intermediate Boc-protected amide was purified by column chromatography and then treated with methanesulfonic acid to produce naphthoindole **4**. On the other hand, heating of 2,3-diamino-1,4-dihydroxyanthraquinone **7** with phenylacetic acid at 170 °C in an inert atmosphere gave anthraimidazole **5** in good yield (Fig. 3; Scheme 2).

3.3. Binding of compounds with AurB

The fluorescence emission was measured to monitor the *in vitro* binding affinity of synthesized compounds **1**–**5** with AurB in the concentration range of 1–200 μM using Tryptophan (Trp) quenching as a probe. Change in emission spectra of tryptophan (Trp) residues (Trp221, Trp257, and Trp326) was observed in response to ligand binding as it affected the environment surrounding the indole ring of Trp in a distance-dependent manner. The maximum tryptophan fluorescence of AurB with ligand occurred between 338 and 340 nm (Fig. 4A1-A5). Binding of the compounds with AurB resulted in shifts of 2–3 nm fluorescence emission maxima to lower wavelength hypsochromic shift or blue shift in a ligand concentration-dependent manner. Such a blue shift of fluorescence peaks occurs when Trp is buried deeper and shielded away from the hydrophobic environment. Change in the microenvironment of Trp residues reveals a conformational change in protein and consequently strength of protein-ligand interaction [63]. The binding of ligands to AurB also decreased the Trp fluorescence intensity in a ligand concentration-dependent manner. This is due to the change in polarity of the Trp environment from polar to nonpolar as it is more buried from the polar environment. Maximum fluorescence intensity at 338 nm (λ_{max}) versus concentrations of ligand was plotted to generate saturation curves for each ligand (Fig. 4B**)** and K_d value for all the compounds determined (Table 2). All the synthesized derivatives were shown to possess improved binding affinity and saturation property even at low concentrations; easily superseding the observed results for parent analog anthrafuran **1**. The observed order of binding affinity of compounds with AurB is in good agreement with the docking results revealing derivative anthrathiophene **2** to possess an enhanced binding profile.

Further, the AMP-PNP competition assay indicated that the quenching of Trp fluorescence (decrease in fluorescence intensity) is more at lower concentration (6.25 μM) of compounds **1**–**5.** On increasing the concentration of the compounds to 25, 50, and 100 μM a decrease in quenching was observed (Supplementary Fig. S4AB and S5A-E). The dissociation constant (K_d) were calculated from the nonlinear, single-site saturation model for each curve (Supplementary Fig. S6). Values of K_d for AMP-PNP in the presence of an increasing concentration of compounds 1–5 increases concomitantly (Supplementary Tables S2 and S3). These results suggest that the K_d value for AMP-PNP increases (or binding affinity decreases) with increasing concentration of compounds 1–5.

3.4. Specificity inferred from real-time binding experiments

To elucidate the real-time binding kinetics in addition to the verification of steady-state affinity (K_d) for synthesized heteroarene-anthraquinone hits, biolayer Interferometry assay (BLI) was performed with purified AurB. The association of each compound with the protein occurring on the surface of the biosensor can be determined by a resultant shift in the wavelength of the sensorgram in real-time. The parent analog anthrafuran **1** was used as the reference control to observe the real-time binding-kinetics and compare the obtained binding affinity of the synthesized compounds **2**–**5** with AurB. The addition of increasing concentrations of compounds **1**–**5** resulted in varied wavelength shifts in the sensorgrams for each compound depicting their differential ability to bind AurB. A significant shift in the association curve in a concentration-dependent manner was detected in the BLI experiments involving anthrathiophene **2** and naphthoindole **4** indicating strong interaction of these synthetic compounds with AurB. A lesser yet reasonable association was detected for the remaining heteroarene-fused anthraquinones hits naphthoisatine **3** and anthraimidazole **5** while parent anthrafuran **1** showed the least binding profile. The real-time binding curves obtained by fitting the data globally to the 1:1 binding model as well as the disassociation constant (K_d) (calculated from the ratio of K_{on} (association) and K_{off} (disassociation) constants) confirmed the robust binding of synthesized hits **(2**–**5)** with AurB. This was evident from their faster association rate and considerably slower dissociation rates as compared to parent anthrafuran **1** (Fig. 5). The results obtained from this experiment were compared with the data from the fluorescence assay results (Table 2).

3.5. AurB activity of the designed compounds by kinase assay

The *in vitro* binding experiment results indicated enhanced binding of the synthesized hits **2**–**5** with AurB as compared to parent anthrafuran **1**. The inhibitory effect of these derivatives was also evaluated in relation to parent anthrafuran **1** to better correlate and estimate their differential potency against AurB. Preceding to assay assessment of the compounds, a kinase titration experiment was performed for AurB which revealed an excellent K_m of 7.7 nM. The difference in the overall activity was observed as a decrease in the kinase activity of AurB. This occurs due to decreased utilization of ATP upon incubation with an increasing concentration of ATP-competitive compounds. This phenomenon was measured through the ADP GLO assay as the resultant decrease of

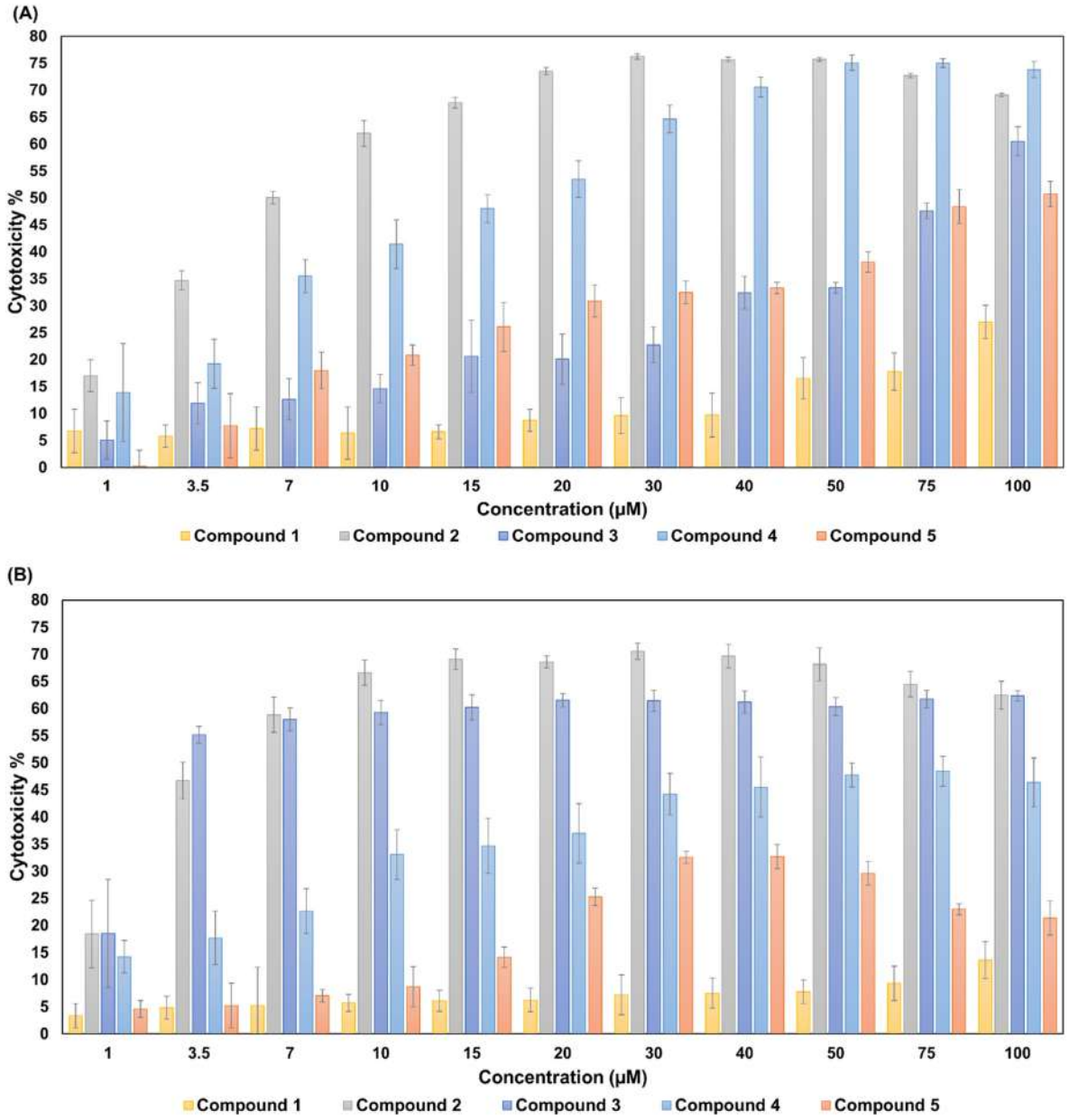

Fig. 7. Cytotoxicity % of compounds 24 h' incubation with (A) Saos-2 and (B) MDA-MB-453 cell line by MTT assay. The assay was performed in 96 well microtiter plates in 6 replicates. The obtained data were analyzed and plotted in the Sigma plot software.

Table 3
Antiproliferative activity (IC_{50}, μM, 24h) of heteroarene-fused anthraquinone derivatives 1–5 against AurB over-expressing MDA-MB-453 and Saos-2 cell lines and noncancerous HEK 293T cell line.

Compounds	IC_{50}, μM		
	MDA-MB-453	Saos-2	HEK 293T
1	>100	>100	>100
2	4.0	7.0	15
3	2.7	79.5	>100
4	>100	15	>100
5	90	>100	>100

luminescence emitted by utilized ATP in the experiment (Fig. 6). Anthrathiophene **2** gave the best IC_{50} of 7.3 μM followed by naphthoindole **4** (17.7 μM), naphthoisatine **3** (29.8 μM), anthraimidazole **5** (33.5 μM) with the least IC_{50} value of 45.7 μM obtained for parent anthrafuran **1**. The IC_{50} in the micromolar range suggests that the compounds are promising lead compounds against AurB and can be taken forward for further structure optimization.

3.6. Antiproliferative potency of the designed heteroarene-fused anthraquinones

Overexpression of AurB has been linked to poor prognosis in several malignant tumors including breast and bone sarcoma [64,65]. Thus, to test the efficacy of synthesized hit compounds **2**–**5** and parent analog anthrafuran **1**, MTT assay was performed with Saos-2 (osteosarcoma) and MDA-MB-453 (breast sarcoma) cell lines. In Saos-2, anthrathiophene **2** showed the highest cytotoxicity in a dose-dependent manner at 24 h' treatment with the IC_{50} value

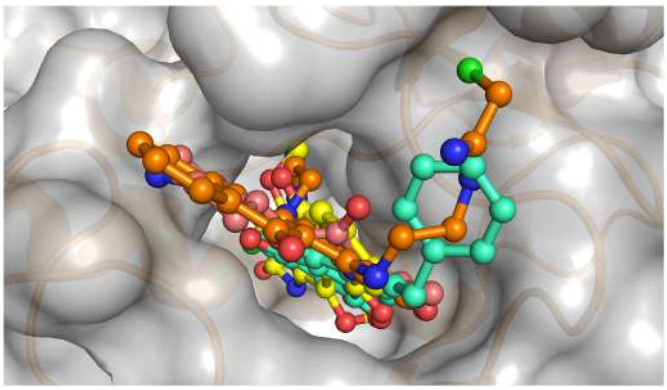

Fig. 8. Superimposition of hit heteroarene-fused anthraquinones (2–5) in the binding pocket of AurB. The superimposed compounds are represented as ball-and-stick with Anthrathiophene 2 (orange); Naphthoisatine 3 (yellow); Naphthoindole 4 (deep salmon) and Anthraimidazole 5 (cyan).

of 7 μM, followed by naphthoindole **4** with IC_{50} of 15 μM. These correlated with the outcome of previous results obtained in this study. Concurrently, naphthoisatine **3**, and anthraimidazole **5** was observed to achieve lesser cytotoxicity in Saos-2 cells with IC_{50} values of 79.5 μM and 90 μM, respectively. Parent compound anthrafuran **1** showed the least cytotoxicity against tested cells and IC_{50} was not reached within the different concentrations used (Fig. 7A).

In MDA-MB-453, naphthoisatine **3** performed best among the rest of the compounds with a better overall IC_{50} value of 2.7 μM with comparable cytotoxicity to anthrathiophene **2** which showed slightly lesser yet significant IC_{50} of 4.0 μM. The IC_{50} for derivatives naphthoindole **4**, anthraimidazole **5**, and parent anthrafuran **1** was not reached, although naphthoindole **4** showed a peak cytotoxicity of 48.4% at 75 μM concentration (Fig. 7B). The resulted IC_{50} values (Table 3) of derivative anthrathiophene **2** correlate well with the experimental values obtained by cell-free ADP Glo-Assay and other *in vitro* techniques forwarding the case of anthrathiophene **2** as a potential effective AurB inhibitor.

The compounds was evaluated further on Human HEK 292T non-cancerous cells (Table 3, Supplementary Fig. S7). The compound anthrathiophene **2** revealed the IC_{50} value of 15 μM which was found to be less than half when compared to 7 μM of Saos-2 and 4 μM of MDA-MB-453. The cytotoxic effect of the parent compound anthrafuran **1** was found to be comparatively higher in these cells as compared to cancerous cells. The other compounds **3**–**5**, displayed comparatively lower cytotoxic effect on HEK 293T compared to cancerous cell lines indicating that these compounds are less toxic to normal cells. Additionally, the specificity of compounds **1**–**5** against cancer cells with different levels of Aurora B expression was estimated with A549 Human lung carcinoma cells which overexpressed AurB gene [66,67] compared to HCT116 human colon carcinoma cell line with median AurB expression [68]. It was observed that derivative **2** exhibited the best binding to Aurora B kinase up to 4 times and inhibited proliferation more efficiently of A549 cells with overexpressed AurB gene (Supplementary Table S4). This indicates that Aurora B kinase could be one of the main targets of anticancer action of heteroarene-fused anthraquinones.

4. Discussion

An intensive study of heterocyclic derivatives annelated to anthraquinone core resulted in the discovery of anthra [2,3-*b*] furan-3-carboxamides, a potent class of antitumor compounds [43]. Among them, the derivative anthrafuran **1** demonstrated a promising multitargeted action on tumor cells, and in particular, inhibited phosphorylation of protein kinase, AurB [69].

The three isoforms of human Aurora kinase (A, B, and C), have a conserved ATP binding pocket [5]. However, there exists a significant difference in the active site residues of AurA and AurB. In AurA, the three active site residues, Leu 215, Thr217 and Arg 220 are substituted with three different residues, Arg159, Glu161, and Lys164 in AurB (Fig. 2A), near the solvent-exposed region of the protein. Various studies have suggested that targeting these residues in the active site can lead to selective inhibition of AurA or AurB [29,70]. It has been demonstrated that in a series of indurubins, aurora kinase sub-type selectivity can be explained by the differential interaction of the inhibitor with Thr217/Glu161 residue [71]. Thus, with the aim to identify novel compounds with enhanced activity and specificity against AurB, a scaffold-hopping approach was adopted based on derivative anthrafuran **1**, which yielded a series of heteroarene-fused anthraquinone derivatives.

Computational screening of virtually modified derivatives of anthrafuran 1 resulted in shortlisting of top four derivatives from molecular docking and MD simulations studies which target AurB (Fig. 1B). The *in silico* results distinctly revealed the promising binding profiles for all the four derivatives which were subsequently synthesized. The prepared compounds experimentally validated the *in silico* findings and established that the designed derivatives possessed better binding affinity than the parent analog anthrafuran **1**. Anthrathiophene **2** demonstrated potent (at submicromolar or low micromolar concentrations) activity in binding and cell-free assays (Table 2). All the studies clearly pinpoint that anthrathiophene **2** is the most potent derivative followed by naphthoindole **4** with naphthoisatine **3** and anthraimidazole **5** exhibiting the least inhibitory potential. These findings are further complemented with the data obtained from AurB over-expressing tumor cell - based MTT assay.

The molecular docking followed by MD simulations reveals that the derivatives bind preferably in the active site of the protein. The docking suggested that the most favorable modifications were those at positions 4 and 11 of ring B and 2 and 3 in the furan ring A. The overall binding mode of the core scaffold is similar in terms of position and orientation in three of the four derivatives 3–5. However, due to the bulky 4,11-bis((2-(chloroacetamidino)ethyl amino substituents at the 4,11-positions, anthrathiophene **2** displayed a slightly different orientation in the active site region of AurB (Fig. 8). The 4,11-side chains of anthrathiophene **2** were observed to orient themselves to maximize the interactions with the protein active site residues. The mode of binding for all the compounds in the active site occurred with minimal conformational perturbations during complexation. The core scaffold of the heteroarene-fused anthraquinone derivatives in the protein-inhibitor complexes is stabilized majorly through hydrogen bonding and hydrophobic interactions. The precise interactions occurring between the compound and AurB play a central role in determining the specificity of each derivative.

Both fluorescence and BLI binding studies demonstrated that compounds **2**–**5** had substantially enhanced K_d values compared to parent anthrafuran **1**. Anthrathiophene **2** displayed the best overall binding profile with AurB. The kinase assays also supported this finding. The better binding of anthrathiophene **2** can be attributed to the strong cation-π interaction of the D benzene ring of the polyannelated core with side-chain nitrogen of Lys164 of AurB. This is further complemented by additional hydrogen-bonded and hydrophobic interactions of its chloroacetamidine-bearing arms with the surrounding amino acid residues as evident from molecular docking and MD simulation studies. Hence, the computational and experimental analyses support each other and are in good

agreement.

These studies underlined the significance of the various substitutions in the modified parent compound anthrafuran **1** whilst reiterating the importance of the hydroxyl groups at the 4,11-positions and the 3-carboxamide moiety of anthra [2,3-*b*]furan-3-carboxamides in their ability to effectively bind at the active site of AurB. The additional modifications of the 3-carboxaaminopyrrolidine moiety of anthrafuran **1** for naphthoindole **4** further augment its inhibition competence. In case of anthrathiophene **2**, the substitution of the 4,11-hydroxyl groups with 2-((chloroacetamidino)ethyl)amines, permits further reorientation in the active site. This enables the formation of necessary stable interactions (Arg159, Glu161, and Lys164) with AurB essential for its potent and selective inhibition. These interactions can be attributed to the observed increased potency of anthrathiophene **2** compared to other derivatives in *in vitro* inhibition of AurB. The large side-chains of anthrathiophene **2** enter and interact inside the groove of the binding pocket of AurB competing with ATP to form strong hydrogen bond and cation-π interactions while concomitantly decreasing the activity of AurB.

5. Conclusion

The present study has potentiated the enhanced binding and inhibition profile of all the four derived hit compounds (2–5) with target AurB as compared to parent analog anthrafuran **1**. Anthrathiophene **2** was found to have excellent inhibition activity in cell-free (ADP Glo Kinase) as well as cell-based (MTT) assays. Hence, targeting AurB by these novel heteroareneanthracenedione lead compounds can prove to be an effective approach to manage the clinical manifestations of various cancers attributed to overexpression of AurB. Overall, our results encourage the use of heteroarene-fused anthraquinone scaffold to design and develop novel therapeutics against AurB.

Declaration of competing interest

The authors report no conflict of interest and also declare no competing financial interest.

Acknowledgments

The work has been carried out as a joint Indian-Russian collaboration funded by DST, India (Int/Rus/RFBR/P-291) and RFBR, Russia (19-33-90179). LM thanks DBT for the grant of fellowship. MAH and MK acknowledge ICMR for research associateship.

Appendix A. Supplementary data

Supplementary data to this article can be found online at https://doi.org/10.1016/j.biochi.2020.12.024.

Author contributions

PK and AES conceptualized the research. MS expressed, purified AurB for *in vitro* experiments and performed the BLI and kinase assays, MK carried out the computational work, MAH conducted the fluorescence binding study, LM performed the MTT assay, AT and VL collected data and synthesized the compounds, ASE and UD planned and supervised experiments, AT, AMK, AES, MS, and PK analyzed the data and co-wrote and revised the manuscript. The manuscript was reviewed and approved by all authors.

References

[1] X. Wang, W. Han, Y. Yu, J. Zhu, R. Zhang, Doxorubicin-induced cardiomyopathy, doxorubicin biosynthesis, Clin. Uses Heal. Implic. (2014) 43–87, https://doi.org/10.1016/j.pcad.2006.10.002.
[2] G. Holmgren, J. Synnergren, Y. Bogestål, C. Améen, K. Åkesson, S. Holmgren, A. Lindahl, P. Sartipy, Identification of novel biomarkers for doxorubicin-induced toxicity in human cardiomyocytes derived from pluripotent stem cells, Toxicology 328 (2015) 102–111, https://doi.org/10.1016/j.tox.2014.12.018.
[3] T. Marumoto, D. Zhang, H. Saya, Aurora-A - a guardian of poles, Nat. Rev. Canc. 5 (2005) 42–50, https://doi.org/10.1038/nrc1526.
[4] P.D. Andrews, E. Knatko, W.J. Moore, J.R. Swedlow, Mitotic mechanics: the auroras come into view, Curr. Opin. Cell Biol. 15 (2003) 672–683, https://doi.org/10.1016/j.ceb.2003.10.013.
[5] M. Carmena, W.C. Earnshaw, The cellular geography of Aurora kinases, Nat. Rev. Mol. Cell Biol. 4 (2003) 842–854, https://doi.org/10.1038/nrm1245.
[6] J.R. Bischoff, G.D. Plowman, The Aurora/Ipl1p kinase family: regulators of chromosome segregation and cytokinesis, Trends Cell Biol. 9 (1999) 454–459, https://doi.org/10.1016/S0962-8924(99)01658-X.
[7] R.D. Carvajal, A. Tse, G.K. Schwartz, Aurora kinases: new targets for cancer therapy. https://doi.org/10.1158/1078-0432.CCR-06-1405, 2006.
[8] N. Matthews, C. Visintin, B. Hartzoulakis, A. Jarvis, D.L. Selwood, Aurora A and B kinases as targets for cancer: will they be selective for tumors?. https://doi.org/10.1586/14737140.6.1.109, 2006.
[9] E. Willems, M. Dedobbeleer, M. Digregorio, A. Lombard, P.N. Lumapat, B. Rogister, The functional diversity of Aurora kinases: a comprehensive review, Cell Div. 13 (2018), https://doi.org/10.1186/s13008-018-0040-6.
[10] S.L. Warner, D.J. Bearss, H. Han, D.D. Von Hoff, Targeting aurora-2 kinase in cancer, Mol. Canc. Therapeut. 2 (2003) 589–595. http://www.ncbi.nlm.nih.gov/pubmed/12813139.
[11] C. Sakakura, A. Hagiwara, R. Yasuoka, Y. Fujita, M. Nakanishi, K. Masuda, K. Shimomura, Y. Nakamura, J. Inazawa, T. Abe, H. Yamagishi, Tumour-amplified kinase BTAK is amplified and overexpressed in gastric cancers with possible involvement in aneuploid formation, Br. J. Canc. 84 (2001) 824–831, https://doi.org/10.1054/bjoc.2000.1684.
[12] H. Zhou, J. Kuang, L. Zhong, W.L. Kuo, J.W. Gray, A. Sahin, B.R. Brinkley, S. Sen, Tumour amplified kinase STK15/BTAK induces centrosome amplification, aneuploidy and transformation, Nat. Genet. 20 (1998) 189–193, https://doi.org/10.1038/2496.
[13] M. Kimura, Y. Matsuda, T. Yoshioka, Y. Okano, Cell cycle-dependent expression and centrosome localization of a third human Aurora/Ipl1-related protein kinase, AIK3, J. Biol. Chem. 274 (1999) 7334–7340, https://doi.org/10.1074/jbc.274.11.7334.
[14] T. Takahashi, M. Futamura, N. Yoshimi, J. Sano, M. Katada, Y. Takagi, M. Kimura, T. Yoshioka, Y. Okano, S. Saji, Centrosomal kinases, HsAIRK1 and HsAIRK3, are overexpressed in primary colorectal cancers, Japanese, J. Canc. Res. 91 (2000) 1007–1014, https://doi.org/10.1111/j.1349-7006.2000.tb00878.x.
[15] N. Keen, S. Taylor, Aurora-kinase inhibitors as anticancer agents, Nat. Rev. Canc. 4 (2004) 927–936, https://doi.org/10.1038/nrc1502.
[16] A. Mortlock, N. Keen, F. Jung, N. Heron, evin Foote, R. Wilkinson, S. Green, Progress in the development of selective inhibitors of aurora kinases, Curr. Top. Med. Chem. 5 (2005) 807–821, https://doi.org/10.2174/1568026054637719.
[17] D. Fancelli, J. Moll, Inhibitors of Aurora kinases for the treatment of cancer, Expert Opin. Ther. Pat. 15 (2005) 1169–1182, https://doi.org/10.1517/13543776.15.9.1169.
[18] F. Girdler, K.E. Gascoigne, P.A. Eyers, S. Hartmuth, C. Crafter, K.M. Foote, N.J. Keen, S.S. Taylor, Validating Aurora B as an anti-cancer drug target, J. Cell Sci. 119 (2006) 3664–3675, https://doi.org/10.1242/jcs.03145.
[19] D. Mahadevan, S. Beeck, Aurora kinase targeted therapeutics in oncology: past, present and future, Expet Opin. Drug Discov. 2 (2007) 1011–1026, https://doi.org/10.1517/17460441.2.7.1011.
[20] H. Yang, T. Burke, J. Dempsey, B. Diaz, E. Collins, J. Toth, R. Beckmann, X. Ye, Mitotic requirement for aurora A kinase is bypassed in the absence of aurora B kinase, FEBS Lett. 579 (2005) 3385–3391, https://doi.org/10.1016/j.febslet.2005.04.080.
[21] P. Chieffi, B. Aurora, A new promising therapeutic target in cancer, Intractable Rare Dis. Res. 7 (2018) 141–144, https://doi.org/10.5582/irdr.2018.01018.
[22] S. Santaguida, C. Vernieri, F. Villa, A. Ciliberto, A. Musacchio, Evidence that Aurora B is implicated in spindle checkpoint signalling independently of error correction, EMBO J. 30 (2011) 1508–1519, https://doi.org/10.1038/emboj.2011.70.
[23] M.J. Kallio, M.L. McCleland, P. Todd Stukenberg, G.J. Gorbsky, Inhibition of Aurora B kinase blocks chromosome segregation, overrides the spindle checkpoint, and perturbs microtubule dynamics in mitosis, Curr. Biol. 12 (2002) 900–905, https://doi.org/10.1016/S0960-9822(02)00887-4.
[24] Z.Z. Lin, Y.M. Jeng, F.C. Hu, H.W. Pan, H.W. Tsao, P.L. Lai, P.H. Lee, A.L. Cheng, H.C. Hsu, Significance of Aurora B overexpression in hepatocellular carcinoma. Aurora B Overexpression in HCC, BMC Canc. 10 (2010), https://doi.org/10.1186/1471-2407-10-461.
[25] R. Sorrentino, S. Libertini, P.L. Pallante, G. Troncone, L. Palombini, V. Bavetsias, D. Spalletti-Cernia, P. Laccetti, S. Linardopoulos, P. Chieffi, A. Fusco, G. Portella,

Aurora B overexpression associates with the thyroid carcinoma undifferentiated phenotype and is required for thyroid carcinoma cell proliferation, J. Clin. Endocrinol. Metab. 90 (2005) 928–935, https://doi.org/10.1210/jc.2004-1518.
[26] V. Bavetsias, S. Linardopoulos, Aurora kinase inhibitors: current status and outlook, Front. Oncol. 5 (2015), https://doi.org/10.3389/fonc.2015.00278.
[27] C. Ditchfield, V.L. Johnson, A. Tighe, R. Ellston, C. Haworth, T. Johnson, A. Mortlock, N. Keen, S.S. Taylor, Aurora B couples chromosome alignment with anaphase by targeting BubR1, Mad 2, and Cenp-E to kinetochores, J. Cell Biol. 161 (2003) 267–280, https://doi.org/10.1083/jcb.200208091.
[28] S. Hauf, R.W. Cole, S. LaTerra, C. Zimmer, G. Schnapp, R. Walter, A. Heckel, J. Van Meel, C.L. Rieder, J.M. Peters, The small molecule Hesperadin reveals a role for Aurora B in correcting kinetochore-microtubule attachment and in maintaining the spindle assembly checkpoint, J. Cell Biol. 161 (2003) 281–294, https://doi.org/10.1083/jcb.200208092.
[29] S. Sarvagalla, M. Coumar, Structural biology insight for the design of sub-type selective aurora kinase inhibitors, Curr. Cancer Drug Targets 15 (2015) 375–393, https://doi.org/10.2174/1568009615666150421110401.
[30] R.W. Wilkinson, R. Odedra, S.P. Heaton, S.R. Wedge, N.J. Keen, C. Crafter, J.R. Foster, M.C. Brady, A. Bigley, E. Brown, K.F. Byth, N.C. Barrass, K.E. Mundt, K.M. Foote, N.M. Heron, F.H. Jung, A.A. Mortlock, F.T. Boyle, S. Green, AZD1152, a selective inhibitor of Aurora B kinase, inhibits human tumor xenograft growth by inducing apoptosis, Clin. Canc. Res. 13 (2007) 3682–3688, https://doi.org/10.1158/1078-0432.CCR-06-2979.
[31] W. Yaoxian, Y. Hui, Z. Yunyan, L. Yanqin, G. Xin, W. Xiaoke, Emodin induces apoptosis of human cervical cancer hela cells via intrinsic mitochondrial and extrinsic death receptor pathway, Canc. Cell Int. 13 (2013), https://doi.org/10.1186/1475-2867-13-71.
[32] K. Fukuhara, S. Oikawa, N. Hakoda, Y. Sakai, Y. Hiraku, T. Shoda, S. Saito, N. Miyata, S. Kawanishi, H. Okuda, 9-Nitroanthracene derivative as a precursor of anthraquinone for photodynamic therapy, Bioorg. Med. Chem. 15 (2007) 3869–3873, https://doi.org/10.1016/j.bmc.2007.03.029.
[33] S. Yeap, M.N. Akhtar, K.L. Lim, N. Abu, W.Y. Ho, S. Zareen, K. Roohani, H. Ky, S.W. Tan, N. Lajis, N.B. Alitheen, Synthesis of an anthraquinone derivative (DHAQC) and its effect on induction of G2/M arrest and apoptosis in breast cancer MCF-7 cell line, Drug Des. Dev. Ther. 9 (2015) 983–992, https://doi.org/10.2147/DDDT.S65468.
[34] J. Gheeya, P. Johansson, Q.R. Chen, T. Dexheimer, B. Metaferia, Y.K. Song, J.S. Wei, J. He, Y. Pommier, J. Khan, Expression profiling identifies epoxy anthraquinone derivative as a DNA topoisomerase inhibitor, Canc. Lett. 293 (2010) 124–131, https://doi.org/10.1016/j.canlet.2010.01.004.
[35] J. Nadas, D. Sun, Anthracyclines as effective anticancer drugs, Expet Opin. Drug Discov. 1 (2006) 549–568, https://doi.org/10.1517/17460441.1.6.549.
[36] S. Raj, V.I. Franco, S.E. Lipshultz, Anthracycline-induced cardiotoxicity: a review of pathophysiology, diagnosis, and treatment, Curr. Treat. Options Cardiovasc. Med. 16 (2014), https://doi.org/10.1007/s11936-014-0315-4.
[37] Z. Nurgalieva, C.C. Liu, X.L. Du, Chemotherapy use and risk of bone marrow suppression in a large population-based cohort of older women with breast and ovarian cancer, Med. Oncol. 28 (2011) 716–725, https://doi.org/10.1007/s12032-010-9512-5.
[38] K.J. Moriarty, H. Koblish, D.L. Johnson, R.A. Galemmo, Progress in the development of agents to control the cell cycle, Top. Med. Chem. (2007) 207–291, https://doi.org/10.1007/7355_2006_006.
[39] M. Yamamoto, A. Takakura, N. Masuda, Next-generation anthracycline for the management of small cell lung cancer: focus on amrubicin, Drug Des. Dev. Ther. (2008) 189–192, https://doi.org/10.2147/dddt.s3972.
[40] R. Shepard, Liposomal annamycin - a new generation anthracycline that overcomes MDR and has No cardiac toxicity for the second line treatment of R/R AML, Clin. Lymphoma, Myeloma & Leukemia 18 (2018), https://doi.org/10.1016/j.clml.2018.07.043. S197–S198.
[41] Anthracyclines in cancer therapy: past, present status and future prospects, Front. Anti-Cancer Drug Discov. (2015) 110–136, https://doi.org/10.2174/9781681081496115060006.
[42] A. Tikhomirov, A. Shtil, A. Shchekotikhin, Advances in the discovery of anthraquinone-based anticancer agents, Recent Pat. Anti-Cancer Drug Discov. 13 (2017), https://doi.org/10.2174/1574892813666171206123114.
[43] A.E. Shchekotikhin, L.G. Dezhenkova, V.B. Tsvetkov, Y.N. Luzikov, Y.L. Volodina, V.V. Tatarskiy, A.A. Kalinina, M.I. Treshalin, H.M. Treshalina, V.I. Romanenko, D.N. Kaluzhny, M. Kubbutat, D. Schols, Y. Pommier, A.A. Shtil, M.N. Preobrazhenskaya, Discovery of antitumor anthra[2,3-b]furan-3-carboxamides: optimization of synthesis and evaluation of antitumor properties, Eur. J. Med. Chem. 112 (2016) 114–129, https://doi.org/10.1016/j.ejmech.2016.01.050.
[44] H. Sun, G. Tawa, A. Wallqvist, Classification of scaffold-hopping approaches, Drug Discov. Today 17 (2012) 310–324, https://doi.org/10.1016/j.drudis.2011.10.024.
[45] Y. Hu, D. Stumpfe, J. Bajorath, Recent advances in scaffold hopping, J. Med. Chem. 60 (2017) 1238–1246, https://doi.org/10.1021/acs.jmedchem.6b01437.
[46] A.E. Shchekotikhin, H.M. Treshalina, M.I. Treshchalin, E.R. Pereverzeva, H.B. Isakova, A.S. Tikhomirov, Experimental evaluation of anticancer efficiency and acute toxicity of anthrafuran for oral administration, Pharmaceuticals 13 (2020) 1–9, https://doi.org/10.3390/ph13050081.
[47] J.M. Elkins, S. Santaguida, A. Musacchio, S. Knapp, Crystal structure of human aurora B in complex with INCENP and VX-680, J. Med. Chem. 55 (2012) 7841–7848, https://doi.org/10.1021/jm3008954.
[48] A.E. Shchekotikhin, V.A. Glazunova, L.G. Dezhenkova, Y.N. Luzikov, V.N. Buyanov, H.M. Treshalina, N.A. Lesnaya, V.I. Romanenko, D.N. Kaluzhny, J. Balzarini, K. Agama, Y. Pommier, A.A. Shtil, M.N. Preobrazhenskaya, Synthesis and evaluation of new antitumor 3-aminomethyl-4,11-dihydroxynaphtho[2,3-f]indole-5,10-diones, Eur. J. Med. Chem. 86 (2014) 797–805, https://doi.org/10.1016/j.ejmech.2014.09.021.
[49] Schrödinger, Maestro | Schrödinger, Schrödinger Release 2018-1, 2018.
[50] ChemAxon, Marvin Sketch. http://Www.Chemaxon.Com/Products/Marvin/, 2013.
[51] N.M. O'Boyle, M. Banck, C.A. James, C. Morley, T. Vandermeersch, G.R. Hutchison, Open babel: an open chemical toolbox, J. Cheminf. 3 (2011), https://doi.org/10.1186/1758-2946-3-33.
[52] Schrödinger, LigPrep | Schrödinger, Schrödinger Release 2018-1, 2018.
[53] R.A. Friesner, R.B. Murphy, M.P. Repasky, L.L. Frye, J.R. Greenwood, T.A. Halgren, P.C. Sanschagrin, D.T. Mainz, Extra precision glide: docking and scoring incorporating a model of hydrophobic enclosure for protein-ligand complexes, J. Med. Chem. 49 (2006) 6177–6196, https://doi.org/10.1021/jm051256o.
[54] L.L.C. Schrödinger, Prime, 2014 version 3.0, New York.
[55] Schrödinger, Schrödinger Release 2018-1, Maest. Interoperability Tools, Desmond Mol. Dyn. Syst., 2018.
[56] A.E. Shchekotikhin, Y.N. Luzikov, Y.B. Sinkevich, V.N. Buyanov, M.N. Preobrazhenskaya, Heterocyclic analogs of 5,12-naphthacenequinone 7*. Synthesis of naphtho-[2,3-f]isatin-5,10-dione derivatives, Chem. Heterocycl. Compd. 44 (2008) 1245–1249, https://doi.org/10.1007/s10593-009-0173-2.
[57] S. Cogoi, S. Zorzet, A.E. Shchekotikhin, L.E. Xodo, Potent apoptotic response induced by chloroacetamidine anthrathiophenediones in bladder cancer cells, J. Med. Chem. 58 (2015) 5476–5485, https://doi.org/10.1021/acs.jmedchem.5b00409.
[58] A.S. Tikhomirov, V.A. Litvinova, Y.N. Luzikov, A.M. Korolev, Y.B. Sinkevich, A.E. Shchekotikhin, Heterocyclic analogs of 5,12-naphthacenequinone 14*. Synthesis of naphtho[2,3-f]indole-3-carboxylic acid derivatives, Chem. Heterocycl. Compd. 53 (2017) 1072–1079, https://doi.org/10.1007/s10593-017-2173-y.
[59] A.E. Shchekotikhin, I.G. Makarov, V.N. Buyanov, M.N. Preobrazhenskaya, Heterocyclic analogs of 5,12-naphthacenequinone. 1. Synthesis of heterocyclic analogs starting from 2,3-diaminoquinizarine, Chem. Heterocycl. Compd. 41 (2005) 914–920, https://doi.org/10.1007/s10593-005-0248-7.
[60] S. Eathiraj, R. Palma, M. Hirschi, E. Volckova, E. Nakuci, J. Castro, C.R. Chen, T.C.K. Chan, D.S. France, M.A. Ashwell, A novel mode of protein kinase inhibition exploiting hydrophobic motifs of autoinhibited kinases: discovery of ATP-independent inhibitors of fibroblast growth factor receptor, J. Biol. Chem. 286 (2011) 20677–20687, https://doi.org/10.1074/jbc.M110.213736.
[61] J. Concepcion, K. Witte, C. Wartchow, S. Choo, D. Yao, H. Persson, J. Wei, P. Li, B. Heidecker, W. Ma, R. Varma, L.-S. Zhao, D. Perillat, G. Carricato, M. Recknor, K. Du, H. Ho, T. Ellis, J. Gamez, M. Howes, J. Phi-Wilson, S. Lockard, R. Zuk, H. Tan, Label-free detection of biomolecular interactions using BioLayer Interferometry for kinetic characterization, Comb. Chem. High Throughput Screen. 12 (2009) 791–800, https://doi.org/10.2174/138620709789104915.
[62] Promega, ADP-glo ™ Kinase Assay, Luminescence, 2009.
[63] P. Sindrewicz, X. Li, E.A. Yates, J.E. Turnbull, L.Y. Lian, L.G. Yu, Intrinsic tryptophan fluorescence spectroscopy reliably determines galectin-ligand interactions, Sci. Rep. 9 (2019), https://doi.org/10.1038/s41598-019-47658-8.
[64] Y. Zhang, C. Jiang, H. Li, F. Lv, X. Li, X. Qian, L. Fu, B. Xu, X. Guo, Elevated Aurora B expression contributes to chemoresistance and poor prognosis in breast cancer, Int. J. Clin. Exp. Pathol. 8 (2015) 751–757.
[65] Z. Zhao, G. Jin, K. Yao, K. Liu, F. Liu, H. Chen, K. Wang, D.R. Gorja, K. Reddy, A.M. Bode, Z. Guo, Z. Dong, Aurora B kinase as a novel molecular target for inhibition the growth of osteosarcoma, Mol. Carcinog. 58 (2019) 1056–1067, https://doi.org/10.1002/mc.22993.
[66] J.J. Yu, L.D. Zhou, T.T. Zhao, W. Bai, J. Zhou, W. Zhang, Knockdown of Aurora-B inhibits the growth of non-small cell lung cancer A549 cells, Oncol. Lett. 10 (2015) 1642–1648, https://doi.org/10.3892/ol.2015.3467.
[67] Z. Xingyu, M. Peijie, P. Dan, W. Youg, W. Daojun, C. Xinzheng, Z. Xijun, S. Yangrong, Quercetin Suppresses Lung Cancer Growth by Targeting Aurora B Kinase, Cancer Med, 2016, https://doi.org/10.1002/cam4.891.
[68] Y.S. Lin, L.J. Su, C.T.R. Yu, F.H. Wong, H.H. Yeh, S.L. Chen, J.C. Wu, W.J. Lin, Y.L. Shiue, H.S. Liu, S.L. Hsu, J.M. Lai, C.Y.F. Huang, Gene Expression Profiles of the Aurora Family Kinases, Gene Expr, 2005, https://doi.org/10.3727/000000006783991962.
[69] Y.L. Volodina, L.G. Dezhenkova, A.S. Tikhomirov, V.V. Tatarskiy, D.N. Kaluzhny, A.M. Moisenovich, M.M. Moisenovich, A.K. Isagulieva, A.A. Shtil, V.B. Tsvetkov, A.E. Shchekotikhin, New anthra[2,3-b]furancarboxamides: a role of positioning of the carboxamide moiety in antitumor properties, Eur. J. Med. Chem. 165 (2019) 31–45, https://doi.org/10.1016/j.ejmech.2018.12.068.
[70] C.O. de Groot, J.E. Hsia, J.V. Anzola, A. Motamedi, M. Yoon, Y.L. Wong, D. Jenkins, H.J. Lee, M.B. Martinez, R.L. Davis, T.C. Gahman, A. Desai, A.K. Shiau, A cell biologist's field guide to aurora kinase inhibitors, Front. Oncol. 5 (2015), https://doi.org/10.3389/fonc.2015.00285.
[71] V. Myrianthopoulos, P. Magiatis, Y. Ferandin, A.L. Skaltsounis, L. Meijer, E. Mikros, An integrated computational approach to the phenomenon of potent and selective inhibition of Aurora kinases B and C by a series of 7-substituted indirubins, J. Med. Chem. 50 (2007) 4027–4037, https://doi.org/10.1021/jm070077z.